EUROPEAN ORGANIZATION FOR NUCLEAR RESEARCH

CERN-SL-2000-011 AP
CERN-NUFACT-NOTE 21

Fringe Fields and Dynamic Aperture in the FNAL Muon Storage Ring

F. Zimmermann, C. Johnstone[*], M. Berz[†], B. Erdelyi[†], K. Makino[†], W. Wan[*]

Abstract

Quadrupole fringe fields can limit the dynamic aperture of muon storage rings. Using the computer code COSY INFINITY for particle tracking and normal-form analysis, we evaluate the importance of fringe fields in the FNAL muon storage ring, and identify the regions of the machine where they are most critical. Dynamic aperture and linear tune shifts with amplitude are calculated considering an ideal machine without any errors or misalignments. We also explore the efficiency of various nonlinear correction schemes, study the momentum acceptance, and evaluate the spin decoherence over the transverse phase space.

Geneva, Switzerland

May 4, 2000

[*]FNAL, Batavia, Illinois, USA.
[†]Michigan State University, East Lansing, Michigan, USA.

1 Introduction

In this note, we investigate the effect of fringe fields in the muon storage ring of the FNAL neutrino factory, continuing earlier studies by M. Berz, K. Makino and B. Erdelyi [1]. The muons only have to be stored for a few hundred turns. Nevertheless, fringe fields are important because the beam fills almost the entire magnet aperture. The transverse normalized beam emittance in the FNAL muon storage ring is 3.2 mm mrad. At 50 GeV, this corresponds to a geometric emittance of about 7 μm, or to beam sizes of a few centimeters. The rms energy spread of 1% rms is also significant. An acceptance of $\pm 3\sigma$ for a few hundred turns is required both in transverse phase space and in momentum.

The FNAL ring optics consists of two arcs separated by two straight sections [2]. One of the straight sections is used for neutrino production. In this straight, the magnets are weakly focusing and the beta functions are large in order to confine the beam divergence. The return straight on the opposite side of the ring exhibits stronger focusing and much smaller beta functions. The magnet apertures vary roughly with the beam size. Quadrupole bore radii are 17 cm in the production straight, 9 cm in the return straight and 7 cm in the arcs. Pole tip fields are 0.05 T, 0.84 T, and 3.6 T, respectively, and quadrupole lengths 3 m in the production sraight and 1 m elsewhere. The arcs are equipped with sextupoles for chromatic correction. Table 1 summarises the relevant parameters. The parameter $\eta_{\rm prod}$ in the table refers to the fraction of muons decaying in the production straight. The exponential decay time of the muons corresponds to about 180 turns.

Table 1: Some parameters of the muon storage ring. † $r_p = 17$ cm in our tracking study

beam energy	E	50 GeV
normalized emittance	$\gamma\epsilon_{x,y}$	3.2 mm rad
rms energy spread	$(\Delta p/p)_{\rm rms}$	1%
circumference	C	1752 m
neutrino decay fraction	$\eta_{\rm prod}$	39.2%
betatron tunes	$\nu_{x,y}$	13.63, 13.31
arc quad radius	r_a	7 cm
arc quad pole tip	$B_{T,a}$	3.6 T
arc quad length	l_a	1 m
arc dipole field	B	6 T
arc dipole length	l	2.4 m
production quad radius	r_p	16.5 cm†
production quad pole tip	$B_{T,p}$	0.05 T
production quad length	l_p	1 m
return quad radius	r_r	9 cm
return quad pole tip	$B_{T,r}$	0.84 T
return quad length	l_r	1 m

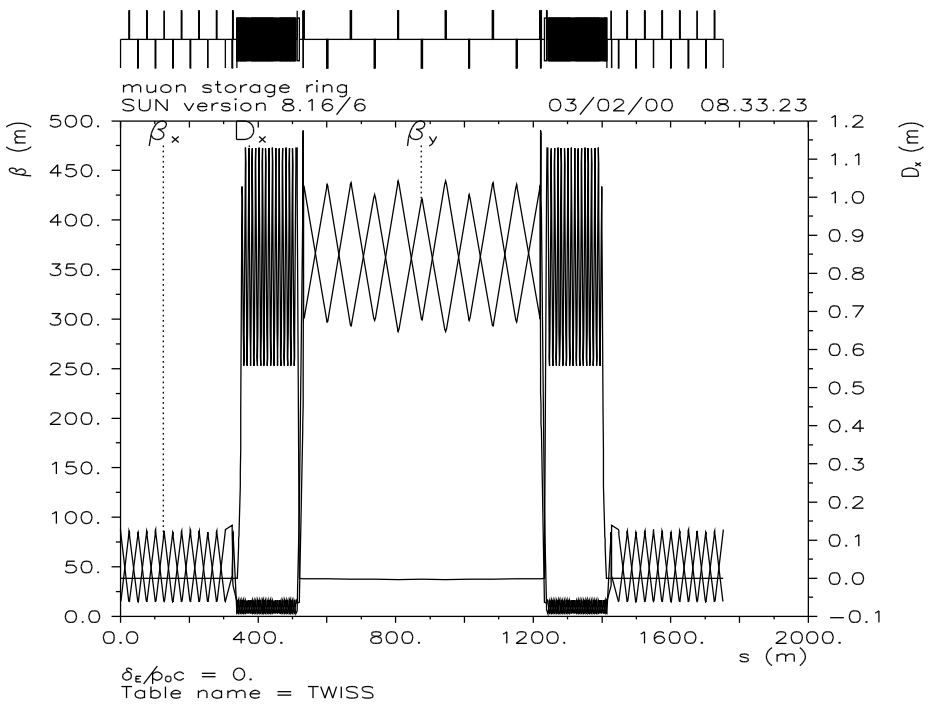

Figure 1: Optics of the FNAL muon storage ring [2].

Figure 2 illustrates the field fall-off near a magnet edge, as assumed in the default fringe-field calculation of COSY INFINITY [3, 4]: The variation with longitudinal position z of the dipole or quadrupole field near the edge of a magnet is represented by an Enge function of the form

$$F(z) = \frac{1}{1 + \exp(a_1 + a_2(z/D) + \ldots + a_6(z/D)^6)} \tag{1}$$

where D denotes the magnet full aperture, and the a_i ($i = 1, \ldots, 6$) are called Enge coefficients. The standard Enge coefficients represent measurements for a family of PEP magnets [5].

2 Results

A COSY input file of the muon storage ring was created from the MAD lattice [6] using the MAD-to-COSY converter [7]. The fractional betatron tunes computed by COSY are $\nu_x = 0.6229$, and $\nu_y = 0.3158$, and agree with the MAD [8] values. In the tracking, three different types of nonlinearities are considered: fringe fields, sextupoles and kinematic corrections.

Figure 3 shows the horizontal and vertical phase space obtained by tracking for 1000 turns (trajectories are plotted on every 5th turn) through a 9th order Taylor map representing the bare ring without fringes and without sextupoles. The vertical axis is the transverse slope of the particle trajectory, x' or y', in units of radian, and the horizontal axis is the transverse position, x or y, in units of meter. The observation point is at the center of a defocusing quadrupole in the return straight. In Fig. 3, the only

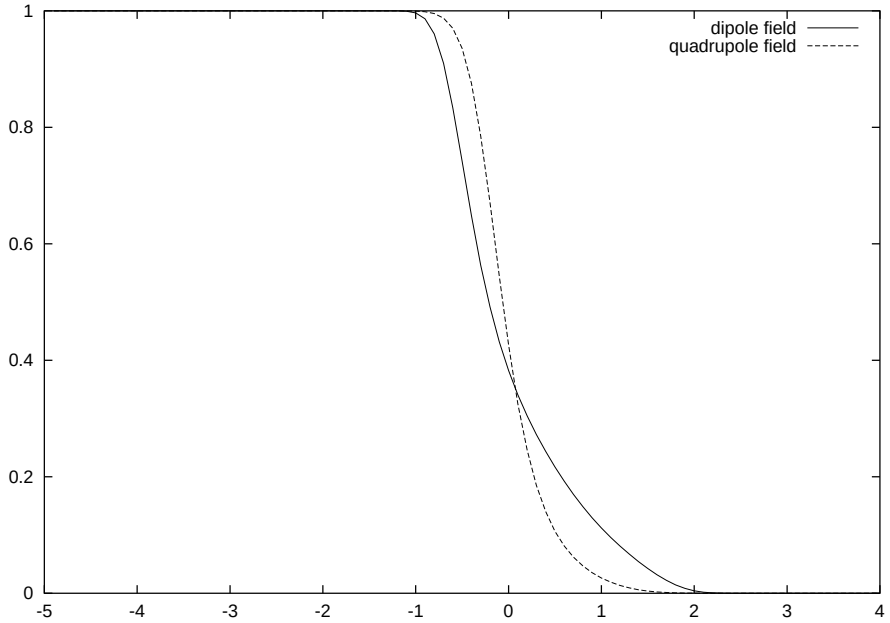

Figure 2: The fall-off of dipole and quadrupole fields assumed in the COSY fringe calulations, as a function of the longitudinal distance from the magnet edge in units of the full magnet aperture. The fall-off is described by an Enge function $F(z)$, as in Eq. (1), with coefficients inferred from PEP magnets [5].

nonlinearity are kinematic terms [9], and the dynamic aperture is far outside the range of the plot, which extends over $\pm 4\sigma$. Figure 4 depicts similar tracking results including the chromatic-correction sextupoles, but still without any fringe fields. This is the situation normally considered in most tracking codes. The dynamic aperture is 3σ or larger. For comparison, Fig. 5 shows the result of a MAD calculation for the same conditions (but trajectories are plotted on every turn). Small differences at large amplitudes can be attributed to the truncation of the Taylor map representation in by COSY.

The dramatic effect of the fringe fields is illustrated in Fig. 6. In this example, the tracking was performed using an option of COSY which automatically corrects the linear effect of the fringe fields (such as tune shift), so that we only observe the influence of the nonlinear terms, and do not need to rematch the linear optics. The plot range in Fig. 6 again covers $\pm 4\sigma$. Now the dynamic aperture is only about $2.5\sigma_x$ in the horizontal plane, and 1.5–$2\sigma_y$ vertically. This falls short of the requirements.

An analytical estimate of the fringe field effect indicates that the linear tune shift induced by quadrupole fringes scales as $\beta^2_{Q;x,y} K_q^2 l_Q$, where K_Q is the quadrupole gradient in units of inverse square meters, l_Q the quadrupole length and β_Q the beta function at the quadrupole [10]. In view of this dependence, we suspected that the aperture reduction is caused by the fringe fields of three or four strong matching quadrupoles (QFF2, QDD2, QMF1, QMD1), located in the matching sections on either side of the production straight. The field gradient in these magnets is up to 500 times higher than the quadrupole gradient in the production straight proper, while the beta functions are of comparable size. Since the magnets are short, we expect that their length could be increased with appropriate optics rematching. In order to estimate the benefit from such a modification, in COSY

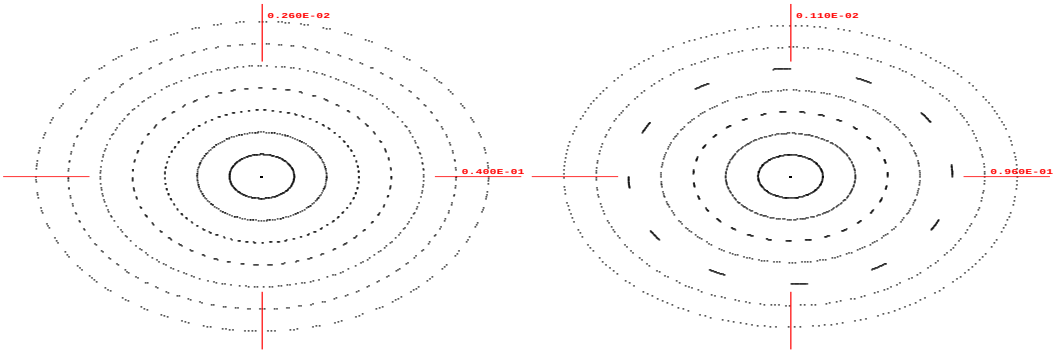

Figure 3: Horizontal (left) and vertical phase space (right), obtained by 9th order tracking through the full muon storage ring, without quadrupole fringe fields and without chromatic-correction sextupoles. Beta functions at the observation point are $\beta_x = 15$ m, $\beta_y = 87$ m. Particles are launched in steps of about 0.5σ, and the plot range extends over about $\pm 4\sigma$. The energy offset is zero.

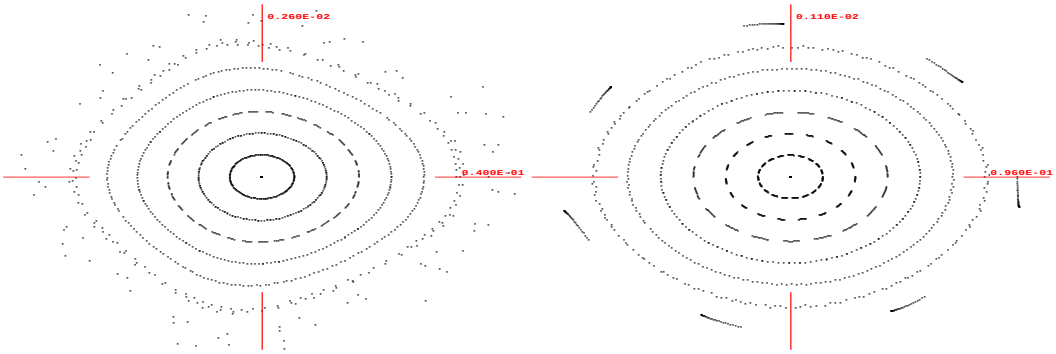

Figure 4: Horizontal (left) and vertical phase space (right), obtained by 9th order tracking with chromatic-correction sextupoles, but without quadrupole fringe fields. Beta functions at the observation point are $\beta_x = 15$ m, $\beta_y = 87$ m. Particles are launched in steps of about 0.5σ, and the plot range extends over about $\pm 4\sigma$. The energy offset is zero.

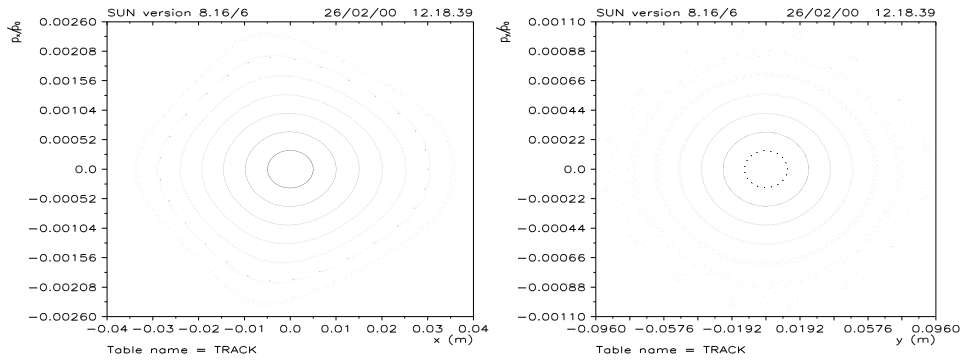

Figure 5: Horizontal (left) and vertical phase space (right), obtained by MAD tracking with chromatic-correction sextupoles, but without quadrupole fringe fields. Beta functions at the observation point are $\beta_x = 15$ m, $\beta_y = 87$ m. Particles are launched in steps of about 0.5σ, and the plot range extends over about $\pm 4\sigma$. The energy offset is zero.

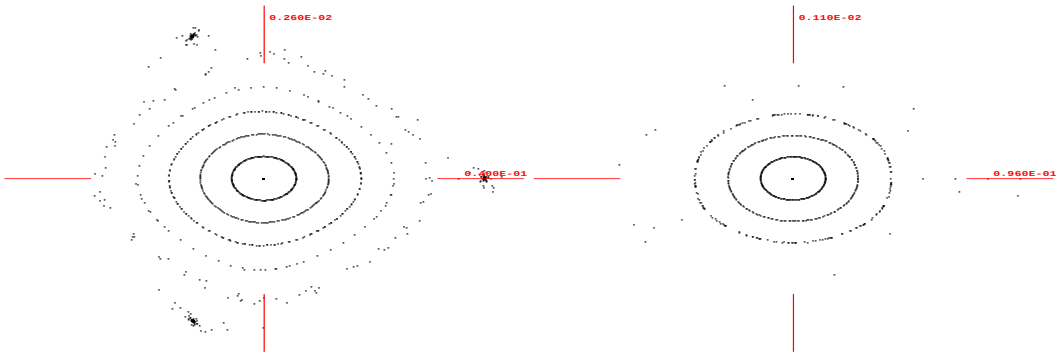

Figure 6: Horizontal (left) and vertical phase space (right), obtained by 9th order tracking through the full muon storage ring, including chromatic-correction sextupoles, and quadrupole fringe fields. Beta functions at the observation point are $\beta_x = 15$ m, $\beta_y = 87$ m. Particles are launched in steps of about 0.5σ, and the plot range extends over about $\pm 4\sigma$. The energy offset is zero.

we can simply switch off the fringe fields for these four magnets, and repeat the previous tracking calculations.

Figure 7 shows the phase space obtained when we ignore the fringe field effects in the matching quadrupoles, but still take fringe fields into account for all the other quadrupoles. The dynamic aperture is about the same as that induced by sextupoles alone, in Fig. 4. Thus, it seems certain that using weaker quadrupoles in the matching section will eliminate the fringe-field problem.

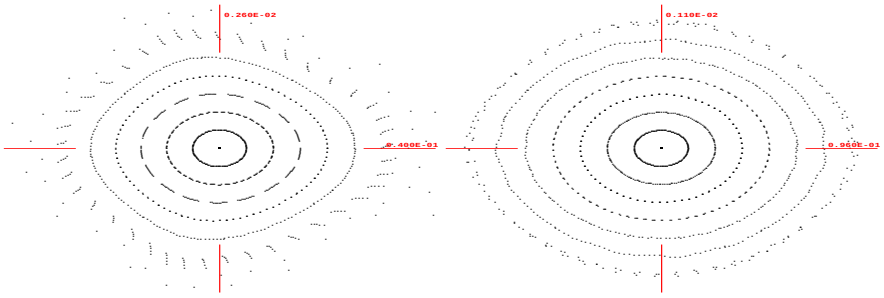

Figure 7: Horizontal (left) and vertical phase space (right), obtained by 9th order tracking through the full muon storage ring with chromatic-correction sextupoles, and with all quadrupole fringe fields, except those in the matching section. Beta functions at the observation point are $\beta_x = 15$ m, $\beta_y = 87$ m. Particles are launched in steps of about 0.5σ, and the plot range extends over about $\pm 4\sigma$. The energy offset is zero.

The tracking accuracy increases with the order of the Taylor map. To examine this dependence, we have tracked through maps of various order representing the most nonlinear case where both sextupoles and all fringe fields are included. Figures 8 and 9 show the phase space obtained with maps of 11th and 7th order, respectively. The dynamic aperture for the 11th order map is similar the 9th order plot in Fig. 6, although there are still some small differences. For the 7th order map, on the other hand, the dynamic aperture is significantly smaller, in both planes. This suggests that the 7th order calculation is not sufficient for the amplitude and turn range of interest. Accordingly, most phase space plots in this report were calculated using maps of order 9 or higher.

The tune shifts with amplitude can be obtained from a COSY normal form analysis. Specifically, the linear tune shift $d\nu_x/dI_x$ is given by the (2 0 0 0) component of the DA vector $\mu(1)$ multiplied by a factor of two, which is due to the choice of normal-form basis vectors in COSY with magnitude $\sqrt{2I}$. Similarly, the quadratic tune shift with amplitude can be obtained from the next-order components of the normal-form tune vector by multiplication with a factor 4.

Linear tune shifts with amplitude (or rather action) for various conditions are listed in Table 2. The table confirms that the fringe fields of the matching quadrupoles are the dominant nonlinear effect. Without these fringes the linear tune shifts are much reduced and the contribution from the sextupoles becomes dominant. This is also reflected by the tune footprints shown in Fig. 10, which were computed by a COSY normal-form analysis and not by tracking. The so-called bare lattice in the last column of Table 2 includes the kinematic correction. Evidently, the kinematic effects are negligible compared with sextupoles and fringe fields.

In an attempt to further optimise the dynamic aperture, we scanned the tunes by ± 0.1 units around

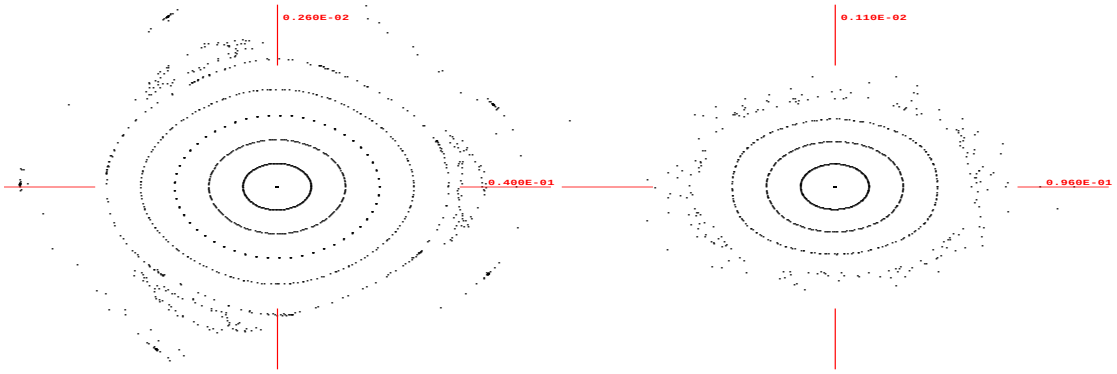

Figure 8: Horizontal (left) and vertical phase space (right), obtained by 11th order tracking through the full muon storage ring, including chromatic-correction sextupoles, and quadrupole fringe fields. Beta functions at the observation point are $\beta_x = 15$ m, $\beta_y = 87$ m. Particles are launched in steps of about 0.5σ, and the plot range extends over about $\pm 4\sigma$. The energy offset is zero.

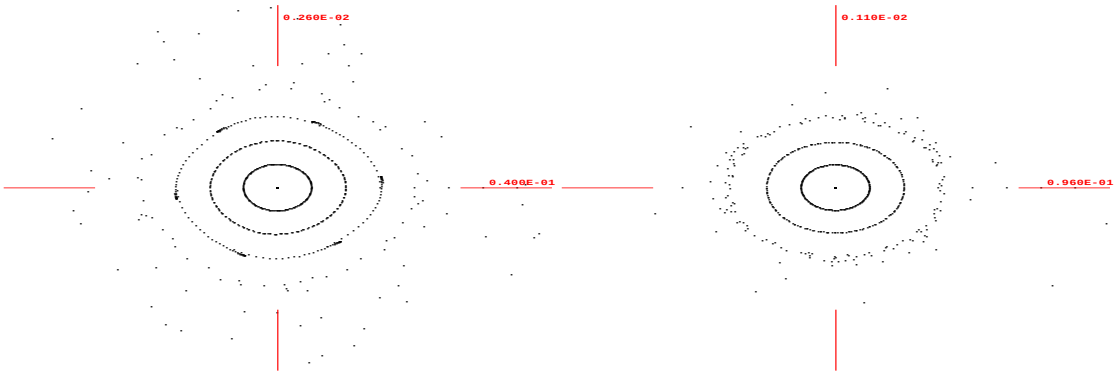

Figure 9: Horizontal (left) and vertical phase space (right), obtained by 7th order tracking through the full muon storage ring, including chromatic-correction sextupoles, and quadrupole fringe fields. Beta functions at the observation point are $\beta_x = 15$ m, $\beta_y = 87$ m. Particles are launched in steps of about 0.5σ, and the plot range extends over about $\pm 4\sigma$. The energy offset is zero.

Table 2: Linear tune shift in various configurations. The bare lattice contains kinematic terms only.

tune shift	$d\nu_x/dI_x$	$d\nu_x/dI_y$	$d\nu_y/dI_y$
sexts. & all fringes	1376	2098	1570
sexts. & fringes w/o matching section	106	-436	82
all fringes, no sexts.	1440	2674	1652
fringes w/o matching section, no sexts.	168	180	146
sexts. only	-4	-558	0.6
bare lattice	60	32	40

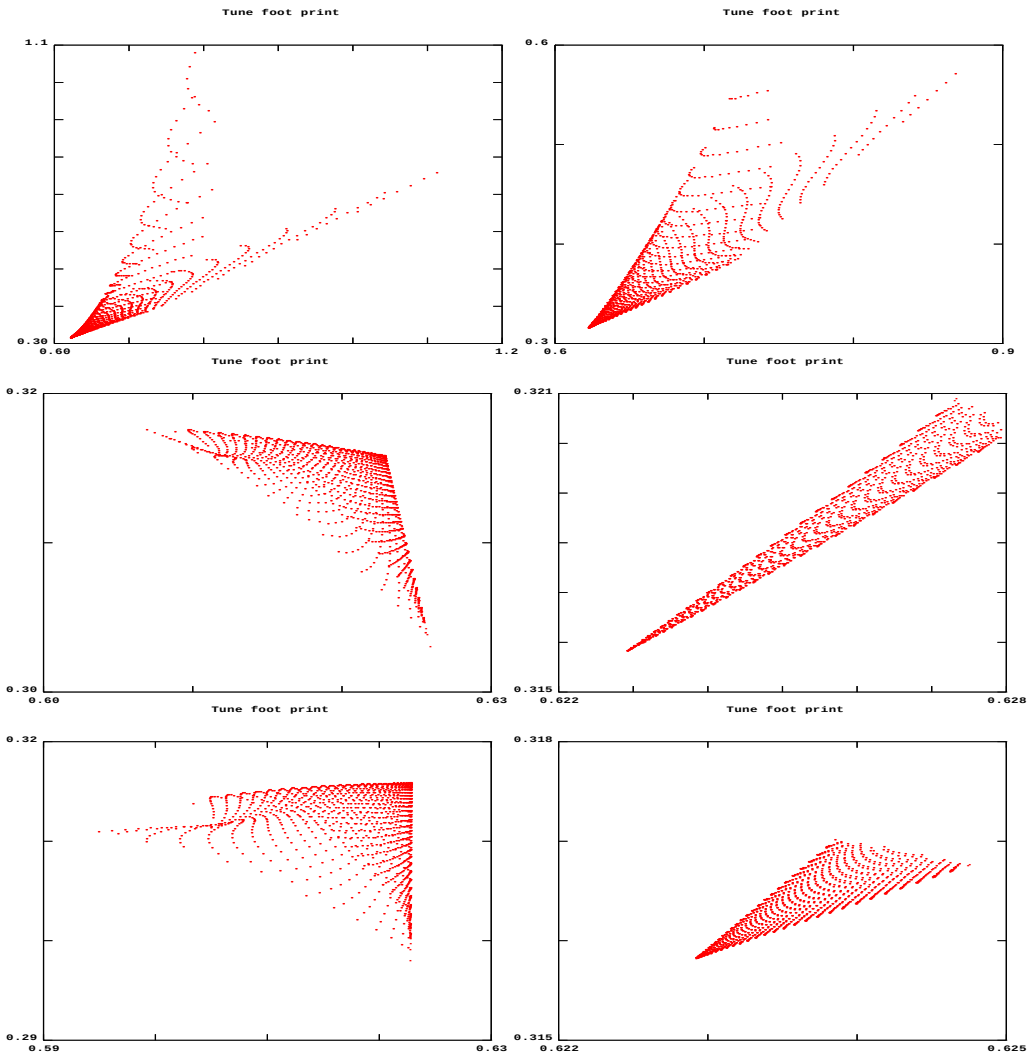

Figure 10: Tune footprints for horizontal and vertical starting amplitudes between 0 and 3σ, calculated from 5th order normal form. In each picture the vertical fractional tune is plotted along the vertical axis, and the horizontal tune along the horizontal. Top left: full lattice including sextupoles and fringes; top right: only fringes; center left: full lattice including sextupoles and all fringes except those in the matching quadrupoles; center right: fringes without matching quadrupoles and no sextupoles; bottom left: only sextupoles; bottom right: bare lattice.

the original working points of 0.623 and 0.316. Figures 11 and 12 show results of 9th order map tracking with sextupoles and fringe fields in straights and arcs, *i.e.*, but not including any fringes in the matching quadrupoles. We observe a rather strong dependence on the tunes, in particular a reduction of the dynamic aperture near the 3rd integer resonance. For the nominal tunes (the far-right picture in the second row) the dynamic aperture is about maximum.

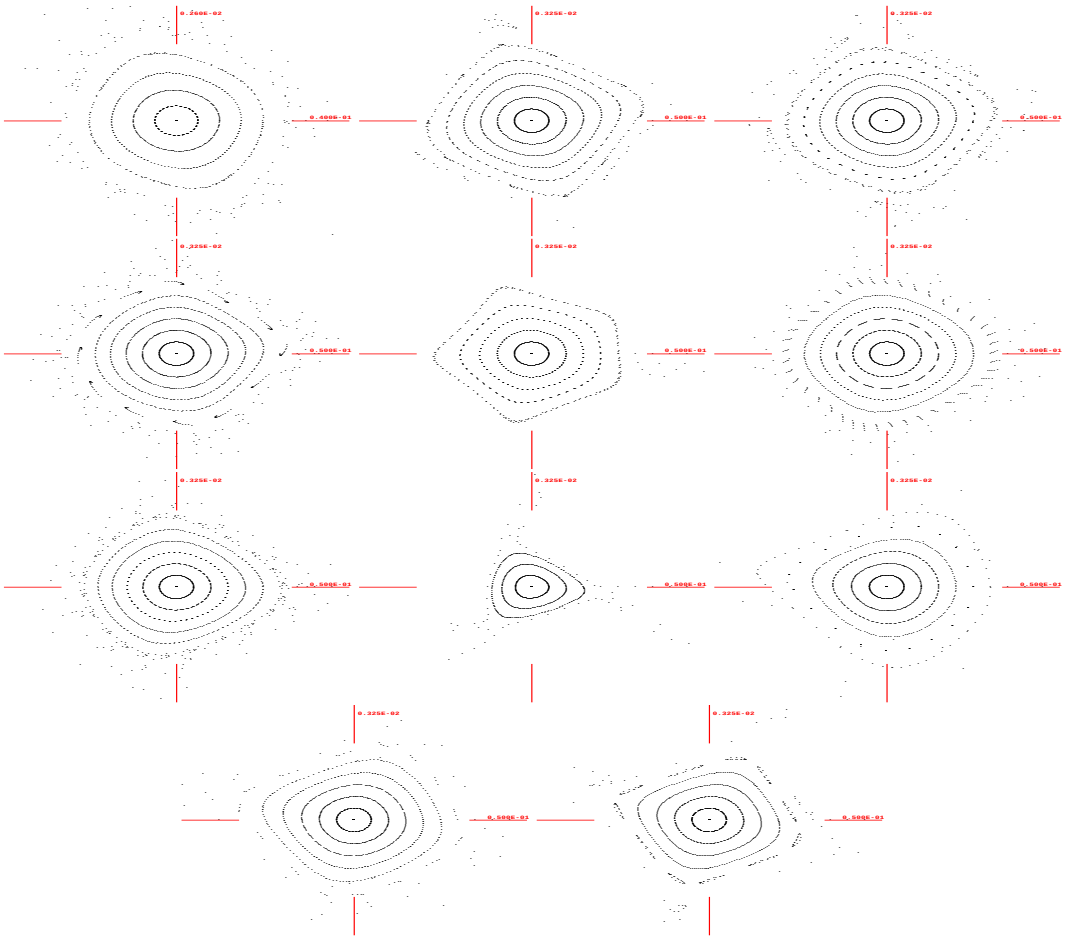

Figure 11: Horizontal phase space with 9th order map including sextupoles and fringe fields (except those in matching quadrupoles) for several values of the horizontal tune, varying from 0.523 (top left) to 0.723 (bottom right) in steps of 0.02. Each plot extends over $\pm 5\ \sigma$.

Octupole correctors can reduce the detuning with amplitude and, thereby, possibly increase the dynamic aperture. An octupole of strength k_o in units of m^{-4}, as defined by MAD, corresponds to a pole-tip field of $B_T = (B\rho)\ k_o a_o^3/6$, where $(B\rho)$ denotes the magnetic rigidity, and a_o the octupole bore radius. In first order perturbation theory, an octupole of strength k_o and length l_o is represented by the nonlinear Hamiltonian

$$H = \frac{k_o l_o}{24}\left[x^4 - 6x^2y^2 + y^4\right], \tag{2}$$

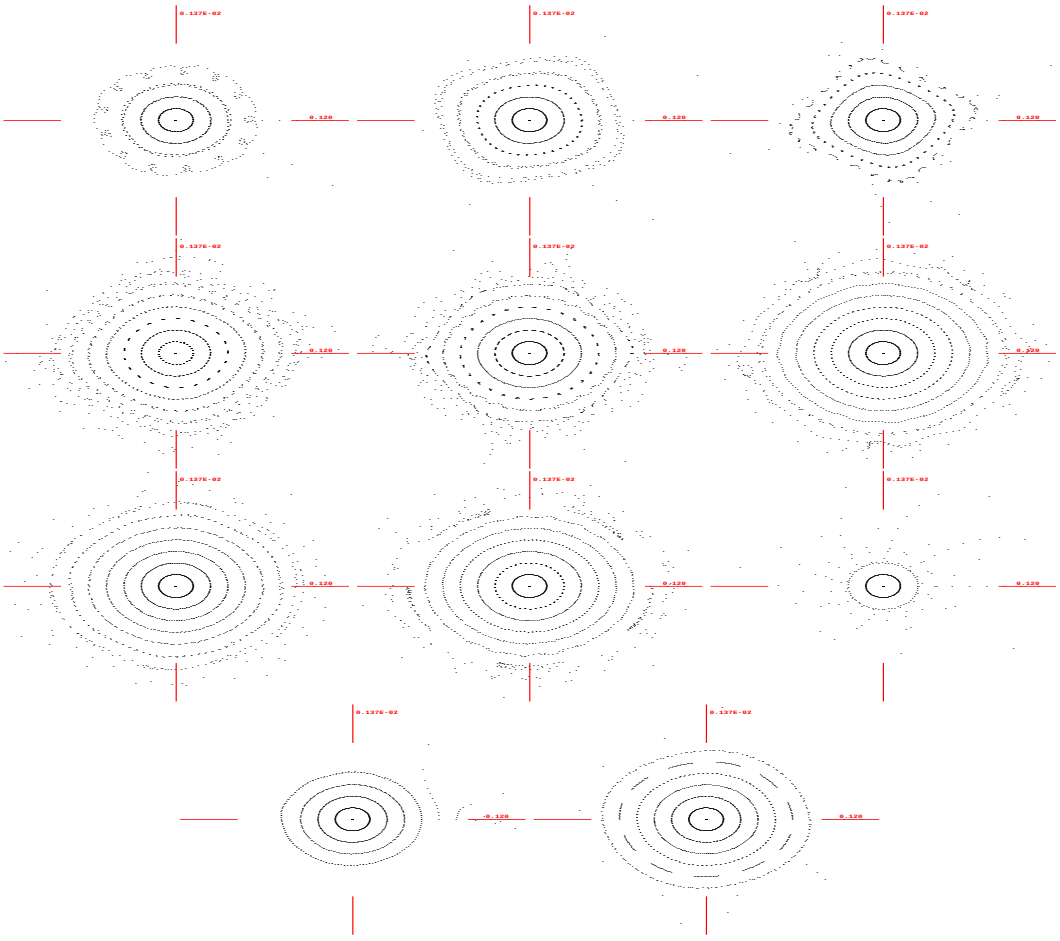

Figure 12: Vertical phase space with 9th order map including sextupoles and fringe fields (except those in matching quadrupoles) for several values of the vertical tune, varying from 0.216 (top left) to 0.416 (bottom right) in steps of 0.02. Each plot extends over $\pm 5\ \sigma$.

and it introduces the amplitude-dependent tune shifts

$$\Delta\nu_x = \frac{1}{2\pi}\frac{k_o l_o}{8}\left[\beta_x^2 I_x - 2\beta_x\beta_y I_y\right] \quad (3)$$

$$\Delta\nu_y = \frac{1}{2\pi}\frac{k_o l_o}{8}\left[\beta_y^2 I_y - 2\beta_x\beta_y I_y\right]. \quad (4)$$

We verified for a single octupole that the DA vector components of the amplitude-dependent tunes obtained from the normal-form analysis in COSY are consistent with the coefficients in Eqs. (3) and (4).

Three octupoles are sufficient to cancel the three linear tune shifts with amplitude. Hence, we positioned three octupoles in the dispersion-three return straight, at a defocusing quadrupole, the adjacent focusing quadrupole, and at the center of the intermediate drift space, respectively. This arrangement does not generate any higher order dispersive components, and, by placing the octupoles at locations with different ratios β_x/β_y we avoid degeneracy. Using COSY, we chose the octupole strengths such that the linear tune shift with amplitude was exactly canceled. The corresponding phase space is shown in Fig. 13. The horizontal dynamic aperture is slightly improved, but the performance in the vertical plane deteriorates.

The nonlinearities may also be corrected by sextupoles, instead of octupoles. Using three sextupoles, we tried to minimise either the linear tune shifts, or, alternatively, the norm of the third order map. These correction attempts were unsuccessful, as the dynamic aperture shrank to almost zero in both transverse planes.

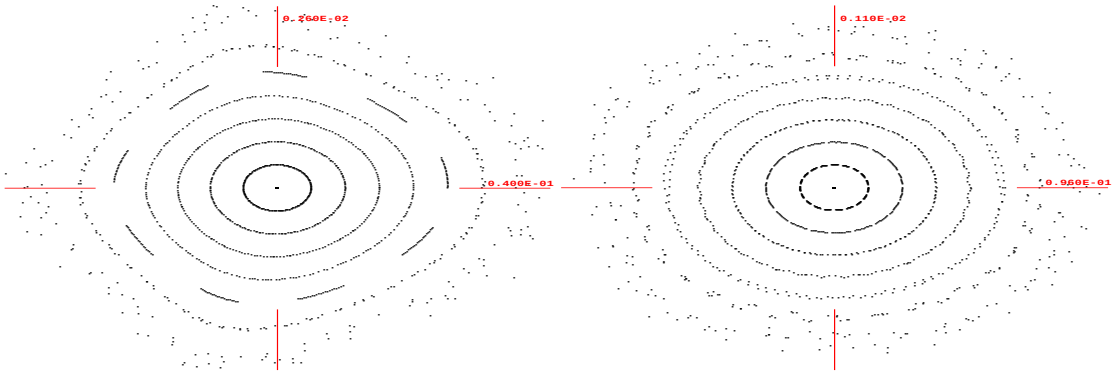

Figure 13: Horizontal (left) and vertical phase space (right), obtained by 9th order tracking through the full muon storage ring, including a set of three octupole correctors which exactly zero the linear tune shift with amplitude, as well as the chromatic-correction sextupoles, and all quadrupole fringe fields, except those in the matching section. Beta functions at the observation point are $\beta_x = 15$ m, $\beta_y = 87$ m. Particles are launched in steps of about 0.5σ, and the plot range extends over about $\pm 4\sigma$. The energy offset is zero.

Another important issue is the dynamic aperture for off-energy particles. We recall that the energy acceptance of the ring should be $\pm 3\%$. Figures 14 and 15 depict the horizontal and vertical phase space, calculated by MAD, for four different energy offsets varying from -3 to $+3\%$. Especially

for large energy offsets, the dynamic aperture decreases strongly. It is essentially zero at an offset of -3%. The blurry character of most trajectories indicates chaotic (potentially unstable) behavior. Figures 16 and 17 depict the equivalent phase space images, obtained from tracking through a 7th order map in three degrees of freedom, using COSY. The additional phase space distortions induced by fringe fields in arcs and straight sections, if any, can be seen in Figs. 18 and 19. Finally, Fig. 20 shows the horizontal phase space for the extreme momentum error of -3% and different values of the horizontal tune, which is varied between 0.6229 and 0.7429. The dynamic aperture is smaller than 1σ for all tune values.

Finally we look at the preservation of polarisation. The spin decoherence caused by different energies can be controlled via momentum compaction factor, rf frequency and rf voltage [11]. The spins can also decohere due to differences in the particle orbits. This second question is addressed in Fig. 21, which displays the variation of the n-axis and the variation in spin tune for trajectories extending up to $\pm 3\sigma$ in transverse phase space. From Fig. 21 we estimate that the net depolarisation due to the dependence of the spin motion on transverse coordinates is considerably less than 1%.

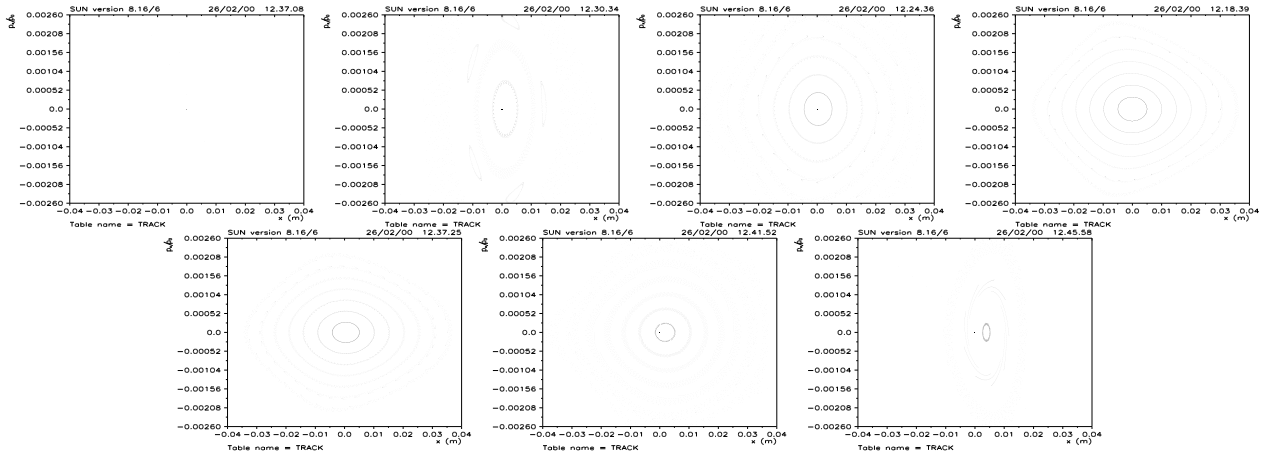

Figure 14: Horizontal phase space for different energy offsets, ranging from -3% to $+3\%$ in steps of 1%, as calculated by MAD. Fringe fields are not included. Each plot extends over $\pm 4\ \sigma$. Every turn is displayed.

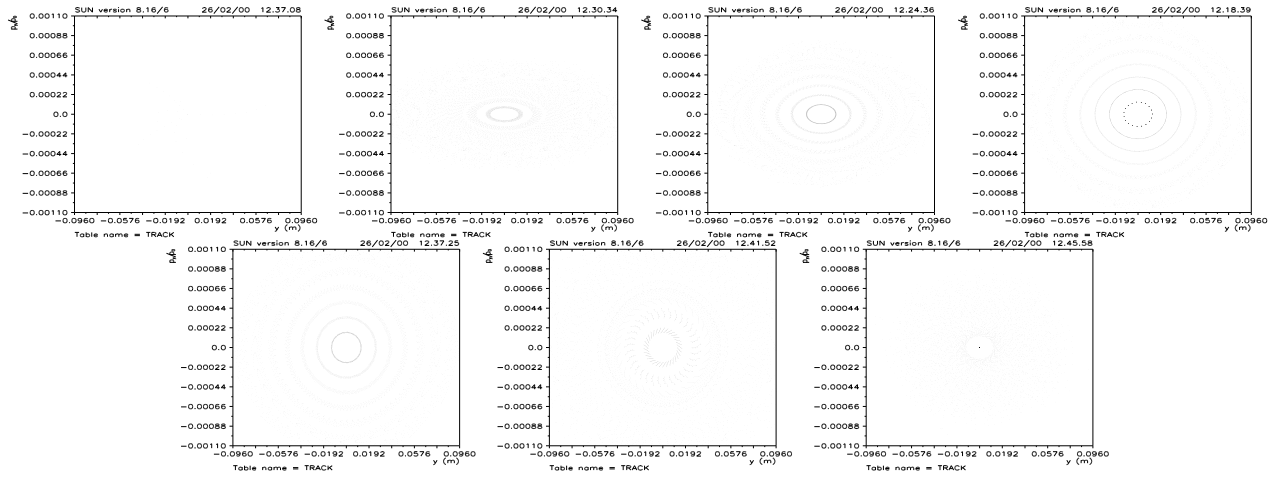

Figure 15: Vertical phase space for different energy offsets, ranging from -3% to $+3\%$ in steps of 1%, as calculated by MAD. Fringe fields are not included. Each plot extends over $\pm 4\ \sigma$. Every turn is displayed.

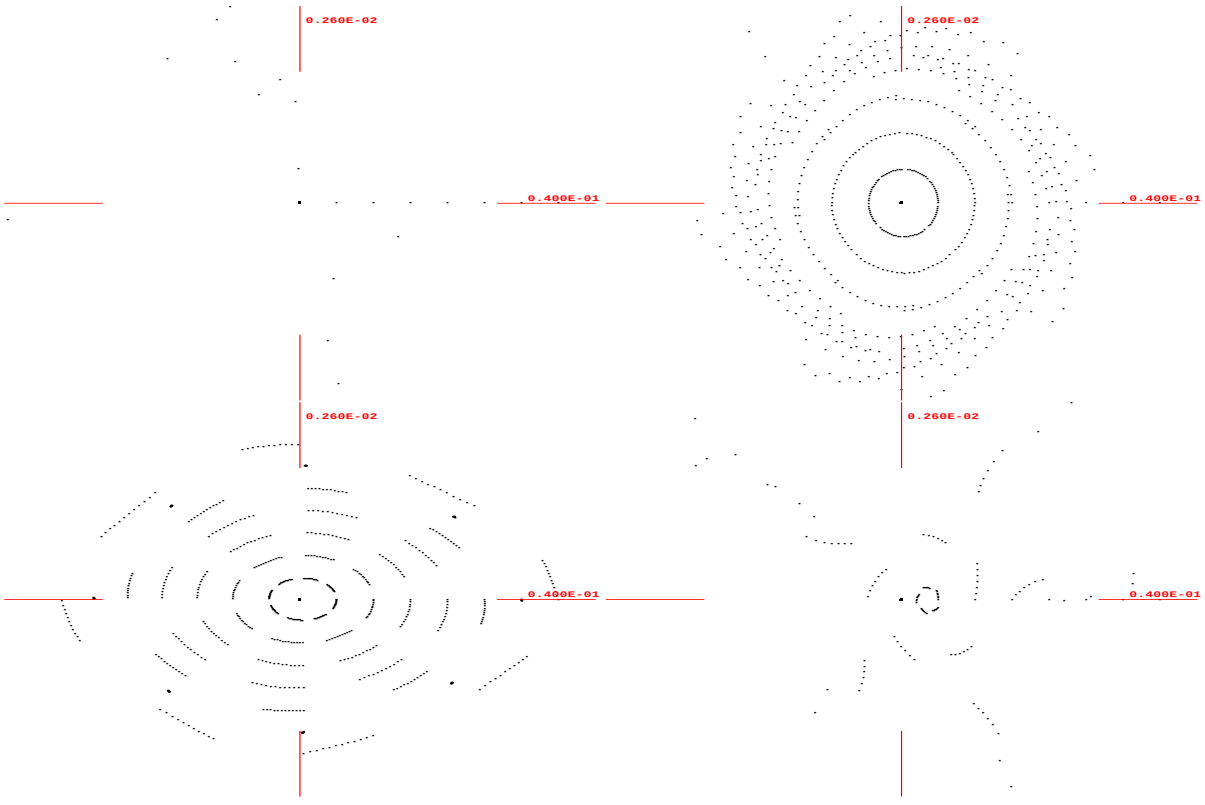

Figure 16: Horizontal phase space for different energy offsets, ranging from -3% to $+3\%$ in steps of 2%, as calculated by 7th order 3-dimensional tracking with COSY. Fringe fields are not included. Each plot extends over $\pm 4\ \sigma$. Every turn is displayed.

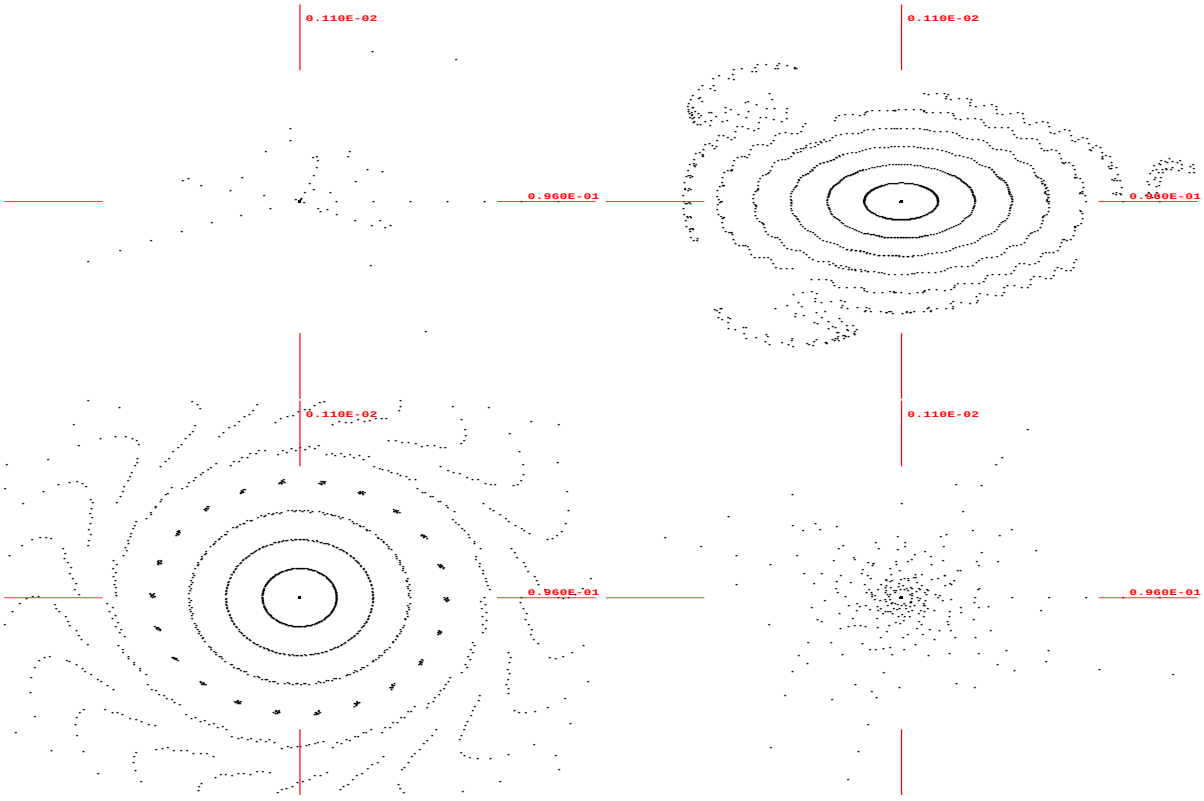

Figure 17: Vertical phase space for different energy offsets, ranging from -3% to $+3\%$ in steps of 2%, as calculated by 7th order 3-dimensional tracking with COSY. Fringe fields are not included. Each plot extends over $\pm 4\ \sigma$. Every turn is displayed.

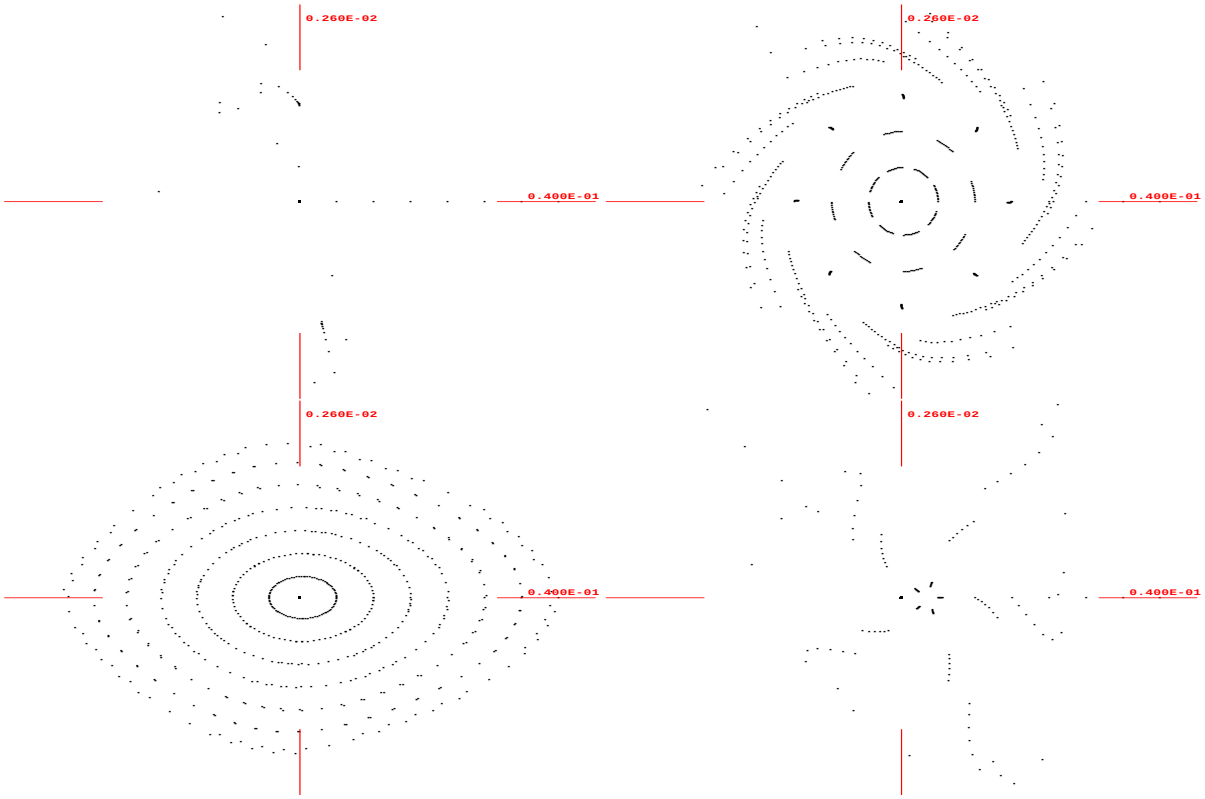

Figure 18: Horizontal phase space for different energy offsets, ranging from -3% to $+3\%$ in steps of 2%, as calculated by 7th order 3-dimensional tracking with COSY. Fringe fields are included except for those in the matching section. Each plot extends over $\pm 4\ \sigma$. Every turn is displayed.

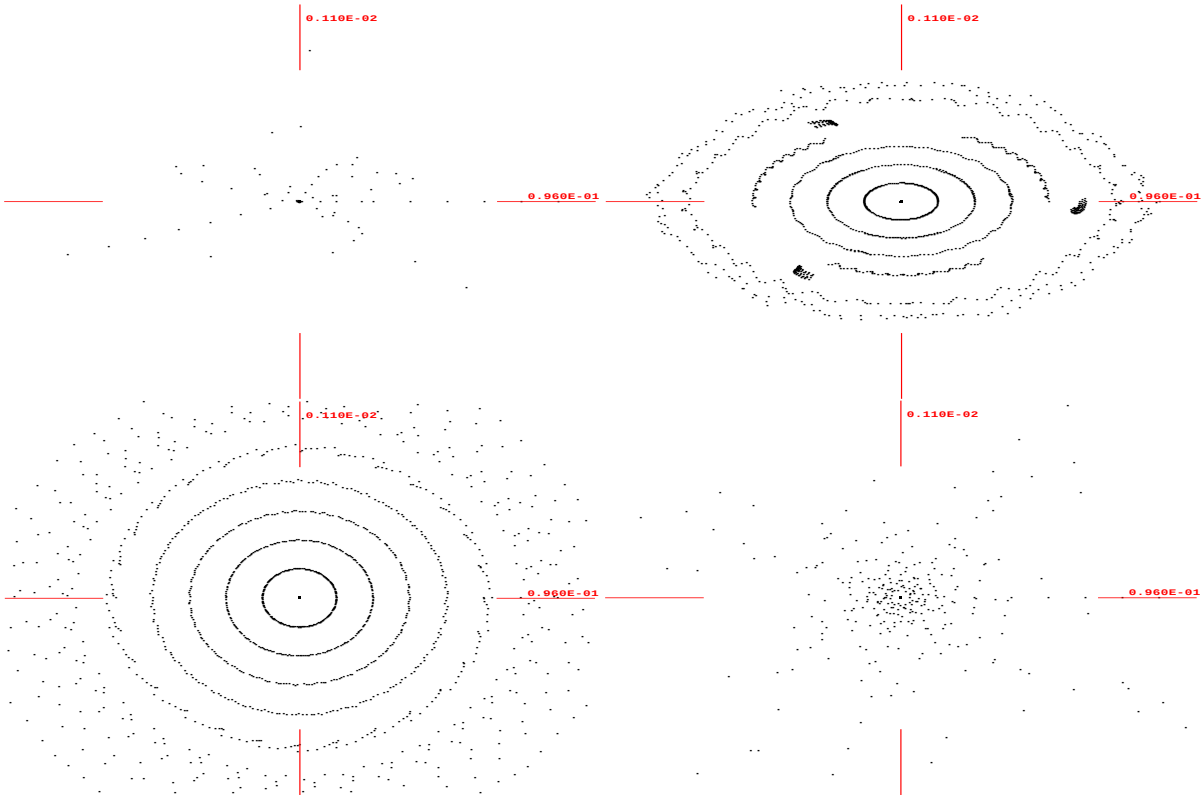

Figure 19: Vertical phase space for different energy offsets, ranging from -3% to $+3\%$ in steps of 2%, as calculated by 7th order 3-dimensional tracking with COSY. Fringe fields are included except for those in the matching section. Each plot extends over $\pm 4\ \sigma$. Every turn is displayed.

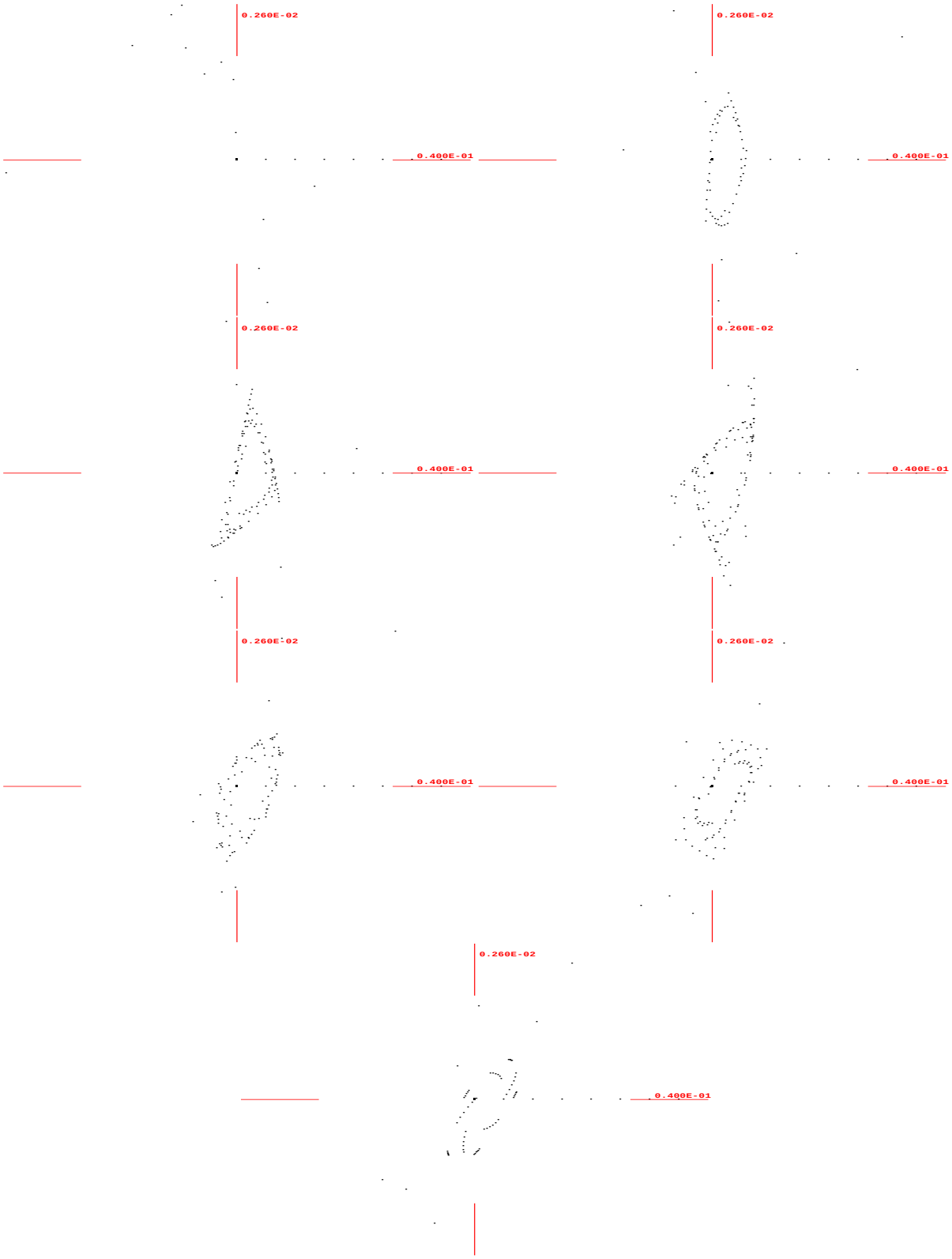

Figure 20: Horizontal phase space for an energy offset of -3% for several values of the horizontal tune, which varies between 0.6229 (top left) and 0.7229 (bottom right) in steps of 0.02. The plots were obtained by 7th order 3-dimensional tracking with COSY. Fringe fields are not included. Each picture extends over $\pm 4\ \sigma$, and every turn is displayed.

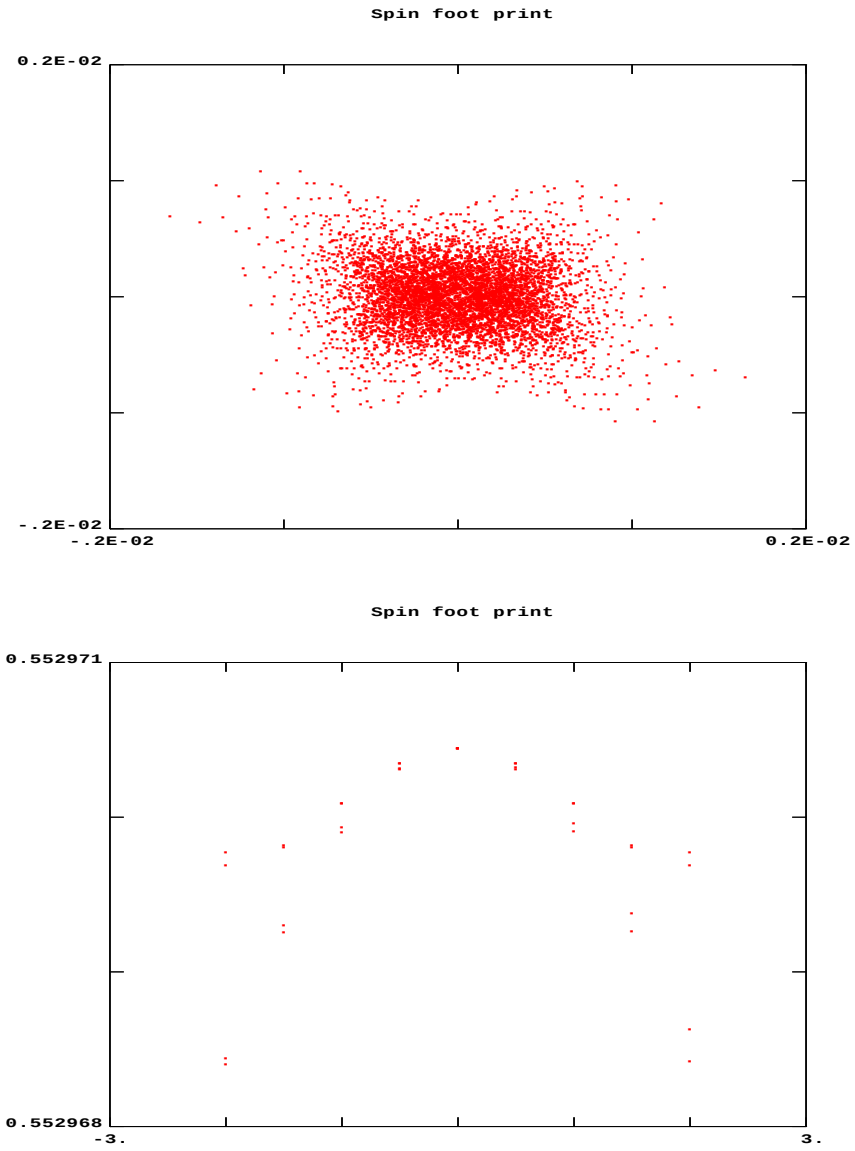

Figure 21: Spin footprints for the FNAL storage ring. Plotted is the longitudinal component of the n-axis versus the horizontal component for transverse coordinates extending up to $\pm 3\sigma$ (top) and the spin tune [the rotation frequency around the n axis, in units of the revolution frequency] as a function of starting coordinates in units of σ (bottom). The spin calculations were performed to 4th order in the transverse coordinates.

3 Conclusions

Quadrupole fringe fields in the matching sections between arcs and production straight reduce the dynamic aperture to about 1.5σ. We expect the problem will be solved by using weaker and longer quadrupoles in these regions. That longer quadrupoles may help was verified for the optics of the CERN muon storage ring, where a similar, but more benign fringe effect was observed [13]. If fringe fields are taken into account only in the rest of the ring, the minimum dynamic aperture exceeds 3σ. It is now dominated by the chromatic-correction sextupoles. Tune scans show that the nominal working point is close to optimum. Still the momentum acceptance appears marginal. Attempts were unsuccessful to improve the performance by adding sextupole or octupole correctors, whose strengths were adjusted so that they either cancelled the tune shift with amplitude or reduced the norm of the Taylor map. Finally, we showed that spin decoherence due to the variation of n axis and spin tune with transverse coordinates will depolarise the muon beam by less than 1%. Most results presented in this report were obtained using the code COSY INFINITY [3, 4].

4 Acknowledgements

We would like to thank N. Holtkamp, E. Keil, and F. Ruggiero for helpful discussions and for encouraging the collaboration. This work was supported in parts by the US Department of Energy under contract No. DE-AC02-76HO3000.

References

[1] M. Berz, K. Makino, B. Erdelyi, "Fringe Field Effects in Muon Rings", Proc. of HEMC'99 workshop on muon colliders at highest energies, Montauk, Long Island (1999).

[2] C. Johnstone, unpublished.

[3] M. Berz et al., COSY INFINITY web page. http://cosy.nscl.msu.edu

[4] K. Makino and M. Berz, "COSY INFINITY version 8", NIM A 427, p. 338 (1999).

[5] K. Brown and J. Spencer, "Non-linear Optics for the Final Focus of the Single-Pass Collider", IEEE Tr. N. Sc. NS-28, 3, p. 2568 (1981).

[6] C. Johnstone, "Large Accetance 50-GeV Muon Storage Ring for Neutrino Production: Lattice Design, CJ2.0" (2000).

[7] The MAD-to-COSY converter was written by R. Servranckx.

[8] H. Grote and F. C. Iselin, "The MAD program (methodical accelerator design) version 8.4: User's reference manual," CERN-SL-90-13-AP-REV.2.

[9] K. Makino and M. Berz, "Effects of Kinematic Correction on the Dynamics in Muon Rings", Proc. of HEMC'99 workshop on muon colliders at highest energies, Montauk, Long Island (1999).

[10] F. Zimmermann, "Tune Shift with Amplitude Induced by Quadrupole Fringe Fields", FNAL Muon Collider Note 94 (2000).

[11] R. Raja, “The effect of RF on polarization in a muon storage ring”, FNAL Muon Collider Note 77 (2000).

[12] E. Keil, private communications, and talk on FNAL work, at ‘~keil/MuMu/Doc/NFWG-/03dec99.pdf’.

[13] F. Zimmermann, “Fringe Fields, Dynamic Aperture, and Transverse Depolarisation in the CERN Muon Storage Ring”, CERN Neutrino Factory Note 2 2 , CERN-SL-2000-012.